



## Reference solution and proportional method to calculate intensity of singular stress field (ISSF) at the interface corner where reinforced fiber enters resin matrix

Nao-Aki Noda , Dong Chen & Yoshikazu Sano

To cite this article: Nao-Aki Noda , Dong Chen & Yoshikazu Sano (2021): Reference solution and proportional method to calculate intensity of singular stress field (ISSF) at the interface corner where reinforced fiber enters resin matrix, Mechanics of Advanced Materials and Structures, DOI: [10.1080/15376494.2021.1882624](https://doi.org/10.1080/15376494.2021.1882624)

To link to this article: <https://doi.org/10.1080/15376494.2021.1882624>



Published online: 18 Feb 2021.



Submit your article to this journal [↗](#)




View related articles [↗](#)



View Crossmark data [↗](#)

# Reference solution and proportional method to calculate intensity of singular stress field (ISSF) at the interface corner where reinforced fiber enters resin matrix

Nao-Aki Noda<sup>a</sup>, Dong Chen<sup>b,a\*</sup> , and Yoshikazu Sano<sup>a</sup>

<sup>a</sup>Department of Mechanical Engineering, Kyushu Institute of Technology, Kitakyushu-shi, Fukuoka, Japan; <sup>b</sup>School of Mechanical and Power Engineering, Zhengzhou University, Zhengzhou, China

## ABSTRACT

To evaluate fiber/matrix bonding properties, the average shear stress is generally used as the interface strength without considering the intensity of singular stress field (ISSF) at the interface ends. In this paper, therefore, how to calculate the ISSF is described in detail at the fiber entry point of the single-fiber under pull-out test. Recent studies showed the ISSF method is quite useful for controlling the debonding strength. As a reference solution, the ISSFs at the fiber entry point are tabulated and illustrated under arbitrary material combination for the specific geometry. By applying the proportional method with this reference solution, the ISSF can be calculated for other geometries conveniently. As an example, the ISSFs of Glass fiber and Carbon fibers are shown to be obtained from the reference solution within 1 percent error. Utilizing those results, the difference between the pull-out test and the micro-bond test is discussed by varying the reinforced fiber properties.

## ARTICLE HISTORY

Received 7 July 2020  
Accepted 25 January 2021

## KEYWORDS

Fiber/matrix interface; fiber pull-out; finite element method; intensity of singular stress field; micro-bond test; proportional method

## 1. Introduction

Fiber reinforced composites is widely used in various fields, based on taking advantage of the high strength and high stiffness of fibers. In fiber reinforced composites, both the fiber and the matrix retain their original physical and chemical identities, yet together they produce a combination of mechanical properties that cannot be achieved with either of the constituents acting alone [1, 2]. To develop new composite manufacturing methods by improving performance requires a better understanding of the role of interface phenomena in the mechanical behavior of these composites [3–5]. Many researchers have been working on fiber pull-out experiments [6–8], but few studies are available for the intensity of singular stress field (ISSF) at the interface ends. The recent studies showed the ISSF method is very useful since the adhesive strength can be expressed as a constant value of the ISSF [9–15]. To calculate the ISSF, a mesh-independent technique named proportional method [16–21] can be applied conveniently by using the same FEM mesh pattern to unknown and reference problems whose exact solution is available by eliminating FEM error [22–24].

A single fiber pull-out test in Figure 1 [8, 25] is widely used to evaluate the interface strength from the average shear stress without considering the singular stress. In the preceding paper, the ISSF was newly studied by varying the fiber embedded length  $l_b$  in pull-out test in Figure 1(a) and

micro-bond test in Figure 2 [26, 27]. As an example, the following conclusion is obtained for Figure 1(b).

1. The crack initiation may start from the buried end Point A in Figure 1(a) when the embedded length  $l_b$  is smaller as  $l_b \leq 150 \mu\text{m}$  for Glass fiber/Epoxy.
2. The crack initiation starts from the fiber entering Point E in Figure 1(a) when the embedded length  $l_b$  is larger as  $l_b \geq 150 \mu\text{m}$  for Glass fiber/Epoxy.

However, this conclusion varies depending on the material combination, for example, if Glass fiber/Epoxy is replaced by Carbon fiber/Epoxy [26]. In this paper, therefore, to calculate the ISSF for specific material combination and specific testing geometry, the reference solution will be provided. This reference solution can be used conveniently to calculate the ISSF at Point E in Figure 1(b) and 2. The reference solution can also be applied to calculating the ISSF of the lap joint in Figure 1(c) coupled with the proportional method [16–21]. This is because Figure 1a–c has the identical singular stress field.

## 2. ISSF Controlling the debonding at the fiber entry point E

The most popular ISSF is known as the stress intensity factor for cracks whose singular stress can be expressed as

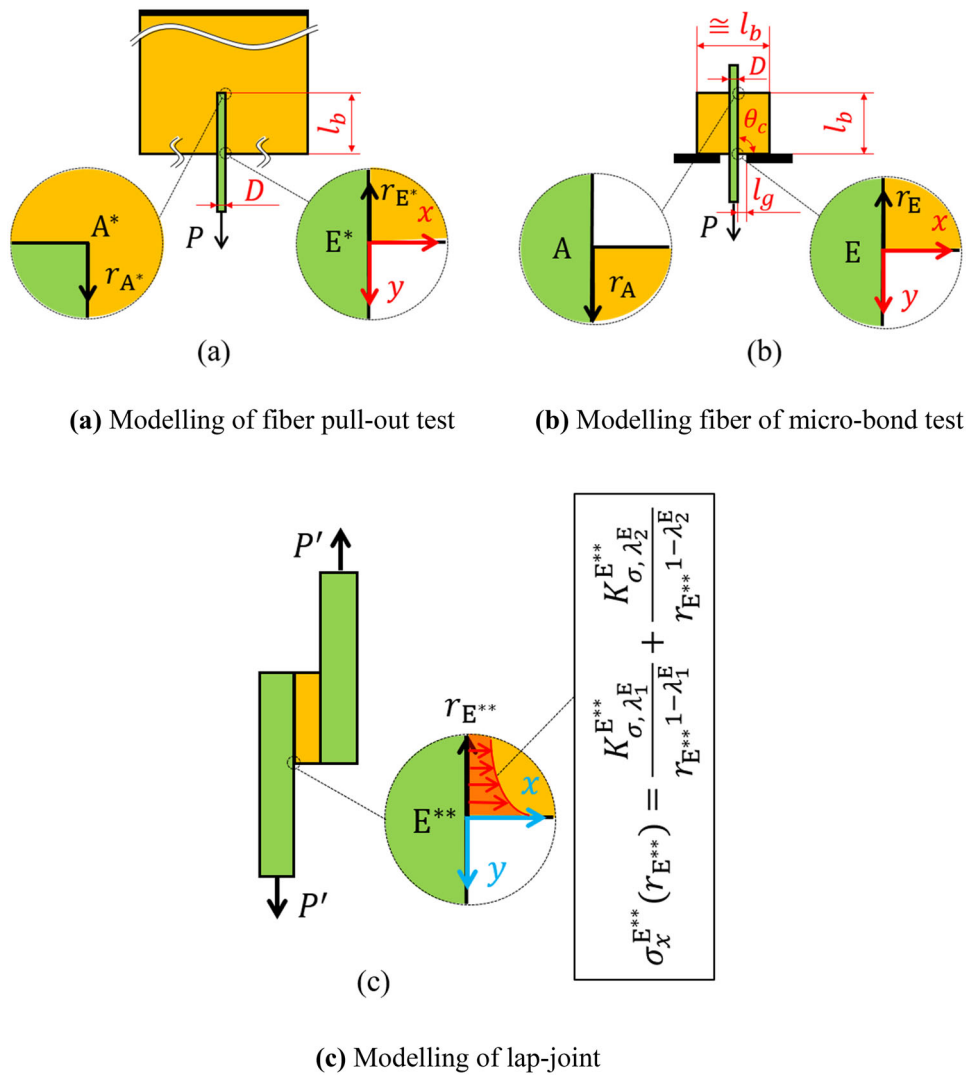


Figure 1. Fiber pull-out test, microbond test and lap joint test having identical singular stress field.

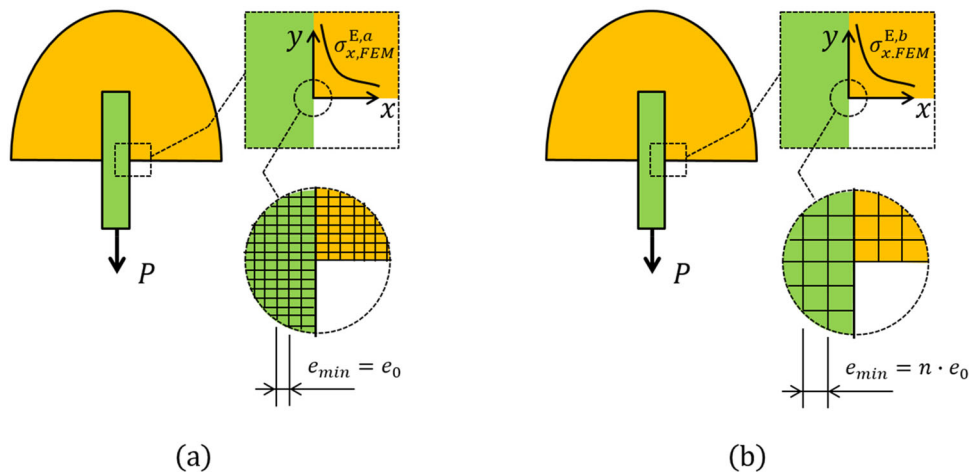


Figure 2. Mesh different model for determining stress distribution of different  $\lambda$ .

$\sigma_x^i \propto 1/r_i^{0.5}$ . The recent studies showed that more general ISSF controlling the interface singular stress  $\sigma_x^i \propto 1/r_i^{1-\lambda}$  in Figure 1 is useful for evaluating the adhesive strength [9–15]. Assuming homogeneous material properties, the singular stress field at Points  $E^{**}$ ,  $E^*$ , A and E can be

expressed as shown in Eq. (1) [28–31]. Here,  $\lambda$  denote singular index determined by solving by solving Eq. (2) [32, 33]. There are two real roots  $\lambda_1$  and  $\lambda_2$  corresponding to two different singular fields for most of the material combinations [34].

$$\sigma_x^i = \frac{K_{\sigma, \lambda_1}^i}{r_i^{1-\lambda_1}} + \frac{K_{\sigma, \lambda_2}^i}{r_i^{1-\lambda_2}}, \quad (i = A, E, E^*) \quad (1)$$

$$\begin{aligned} & 4 \sin^2(\pi\lambda) \left\{ \sin^2\left(\frac{\pi\lambda}{2}\right) - \lambda^2 \right\} \beta^2 + 4\lambda^2 \sin^2(\pi\lambda) \alpha \beta \\ & + \left\{ \sin^2\left(\frac{\pi\lambda}{2}\right) - \lambda^2 \right\} \alpha^2 + 4\lambda^2 \sin^2(\pi\lambda) \beta \\ & + 2 \left\{ \lambda^2 \cos(2\pi\lambda) + \sin^2\left(\frac{\pi\lambda}{2}\right) \cos(\pi\lambda) + \frac{1}{2} \sin^2(\pi\lambda) \right\} \alpha \\ & + \sin^2\left(\frac{3\pi\lambda}{2}\right) - \lambda^2 = 0 \end{aligned} \quad (2)$$

Here,  $\alpha$  and  $\beta$  denote bimaterial parameters of Dundurs [35] defined by Eq. (3). Real material combinations among metal, ceramics, resin, and glass are provided by Suga et al. [36] and Yuuki [37] in the  $\alpha - \beta$  space. For the Carbon/Epoxy material combination,  $\alpha = 0.9775$ ,  $\beta = 0.2250$ ,  $\lambda_1 = 0.6751$ ,  $\lambda_2 = 0.9999$ .

$$\begin{aligned} \alpha &= \frac{G_F(\kappa_M + 1) - G_M(\kappa_F + 1)}{G_F(\kappa_M + 1) + G_M(\kappa_F + 1)}, \quad \beta = \frac{G_F(\kappa_M - 1) - G_M(\kappa_F - 1)}{G_F(\kappa_M + 1) + G_M(\kappa_F + 1)}, \\ \kappa_i &= \begin{cases} (3 - \nu_i)/(1 + \nu_i) & (\text{Plain stress}) \\ (3 - 4\nu_i) & (\text{Plain strain}) \end{cases} \quad (i = M, F) \end{aligned} \quad (3)$$

The debonding stress  $\sigma_x^i$  is controlled by the ISSFs  $K_{\sigma, \lambda_1}$ ,  $K_{\sigma, \lambda_2}$ ; and therefore, the debonding stress  $\sigma_x^i$  can be larger when the ISSFs  $K_{\sigma, \lambda_1}$ ,  $K_{\sigma, \lambda_2}$  are larger. Note that the debonding stress  $\sigma_x^i$  can be also larger when the singular indexes  $\lambda_1$  and  $\lambda_2$  are smaller because of the stress singularity in Eq. (1). Under the fixed geometry, the ISSFs  $K_{\sigma, \lambda_1}$ ,  $K_{\sigma, \lambda_2}$  and the singular indexes  $\lambda_1$  and  $\lambda_2$  vary depending on the material combination.

### 3. Reference solution and proportional method to calculate the ISSF at fiber entry point

The singular stress fields at the interface end at Point E\* in Figure 1(a) and Point E in Figure 1(b) are identical with the singular stress field of the lap joint in Figure 1(c) [32, 36]. The ISSFs of these problems can be obtained conveniently by using the proportional method [16–21] if one of the ISSF is known under the specific material combination.

Finite element method (FEM) analysis should be well conducted and may require experience and skills for engineering applications [38–46]. In this analysis, a mesh independent proportional method is used to calculate the ISSF  $K_{\sigma}^i$  defined in Eq. (1). For resin matrix with reinforced fiber, second singular index  $\lambda_2$  is close to 1; therefore, the second term of ISSF can be omitted. Then, the ISSF can be calculated from the ratio of FEM stress  $\sigma_{x, FEM}^i(r_i)$  as shown in Eq. (4), it can be verified that the FEM stress ratios obtained by this method is independent of mesh size [16, 20, 32, 33]. When the second term of ISSF cannot be omitted, Miyazaki et al. [20, 21] proposed a proportional method obtaining two distinct stress distributions by using two same scale model with different mesh sizes.

Figure 2 shows two fiber pull-out model of the same scale. The model as shown in Figure 2(a) has minimum elements  $e_{min} = e_0$  at the vicinity of Point E\* and the model as shown in Figure 2(b) has minimum elements  $e_{min} = n \cdot e_0$  there. The FEM stress of the model (a) is denoted by  $\sigma_{x, FEM}^{E, a}(r_0)$ , and  $r_0$  denote the distance from the corner edge Point E\* in Figure 1(a). Similarly,  $\sigma_{x, FEM}^{E, b}(n \cdot r_0)$  denotes the FEM stress of the model (b) at distance  $n \cdot r_0$ . The stress distribution for model (a) corresponding with  $\lambda_1$  and  $\lambda_2$  can be obtained by Eq. (5) [20, 21].

$$\begin{aligned} \frac{K_{\sigma, \lambda_1, i}}{K_{\sigma, \lambda_1, j}} &= \frac{\sigma_{x, \lambda_1, i}^{FEM}(r_i)}{\sigma_{x, \lambda_1, j}^{FEM}(r_j)}, \quad (i, j = A, E, E^*) \\ \frac{K_{\sigma, \lambda_2, i}}{K_{\sigma, \lambda_2, j}} &= \frac{\sigma_{x, \lambda_2, i}^{FEM}(r_i)}{\sigma_{x, \lambda_2, j}^{FEM}(r_j)}, \quad (i, j = A, E, E^*) \end{aligned} \quad (4)$$

$$\begin{cases} \sigma_{FEM, \lambda_1}^{E, a}(r_0) = \frac{\sigma_{x, FEM}^{E, a}(r_0)}{1 - n^{\lambda_1 - \lambda_2}} - \frac{\sigma_{x, FEM}^{E, b}(n \cdot r_0)}{n^{\lambda_2 - 1} - n^{\lambda_1 - 1}} \\ \sigma_{FEM, \lambda_2}^{E, a}(r_0) = \frac{\sigma_{x, FEM}^{E, a}(r_0)}{1 - n^{\lambda_2 - \lambda_1}} + \frac{\sigma_{x, FEM}^{E, b}(n \cdot r_0)}{n^{\lambda_2 - 1} - n^{\lambda_1 - 1}} \end{cases} \quad (5)$$

When the single fiber pull-out tests in Figure 1(a) is used to investigate the interface strength, the debonding strength should be smaller than the tensile strength of the fiber. Therefore, high adhesion systems require very small embedding lengths  $l_b (< 100\mu\text{m})$  [2]. To find out suitable testing condition the ISSFs have to be calculated by varying the geometry under the specified fiber property. In the previous study [26], the reference solution was provided to calculate the ISSF at the fiber entry point E\*'', the symbol should similar to that of A\*. In this study, to calculate the ISSF at the fiber entry point, the reference solution is provided under arbitrary material combinations by using the reciprocal work contour integral method (RWCIM) described in the Appendix A. Since the singular index varies depending on the fiber/matrix material combination, the ISSF is normalized as shown in Eq. (6).

$$\begin{aligned} F_{\sigma, \lambda_1} &= K_{\sigma, \lambda_1} / \left[ (P/D)(D/2)^{1-\lambda_1} \right] \\ F_{\sigma, \lambda_2} &= -K_{\sigma, \lambda_2} / \left[ (P/D)(D/2)^{1-\lambda_2} \right] \end{aligned} \quad (6)$$

Then, the normalized ISSFs are shown in the  $\alpha - \beta$  space under fixed fiber embedding length  $l_b/D = 5$ .

Figure 3 and Table 1 illustrates the normalized ISSF  $F_{\sigma, \lambda_1}$  by varying  $\alpha$ ,  $\beta$ . The value of singular index  $\lambda_1$  is shown in Table 3. A material combination for Carbon fiber/Epoxy ( $\alpha = 0.9775$ ,  $\beta = 0.2250$ ,  $\lambda_1 = 0.6751$ ) discussed in our previous study [26, 27] can be plotted in Figure 3 as  $F_{\sigma, \lambda_1} = 0.164$ . Then, when  $D = 20\mu\text{m}$ ,  $l_b = 100\mu\text{m}$ , and  $P = 1\text{MPa} \cdot 20\mu\text{m} \cdot 1\text{mm} = 0.02\text{N}$ , we have  $K_{\sigma, \lambda_1} = 0.346\text{MPa} \cdot m^{1-0.6751}$ . Another material combination for or Glass fiber/Epoxy ( $\alpha = 0.9071$ ,  $\beta = 0.2016$ ,  $\lambda_1 = 0.6592$ ) can be plotted in Figure 3 as  $F_{\sigma, \lambda_1} = 0.198$ . When  $D = 20\mu\text{m}$ ,  $l_b = 100\mu\text{m}$  and  $P = 1\text{MPa} \cdot 20\mu\text{m} \cdot 1\text{mm} = 0.02\text{N}$ , we have  $K_{\sigma, \lambda_1} = 0.433\text{MPa} \cdot m^{1-0.6592}$ .

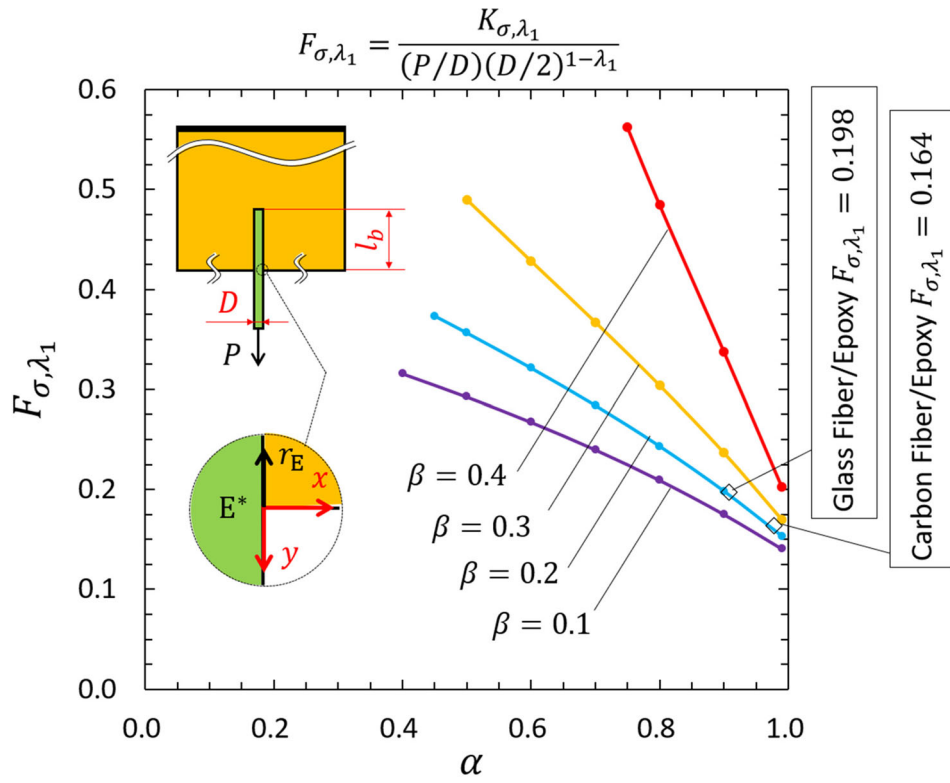


Figure 3.  $F_{\sigma,\lambda_1}$  at the fiber entry point  $E^*$  in pull-out test in Figure 1(a) when  $l_b/D = 5$ .

Table 1.  $F_{\sigma,\lambda_1}$  in Figure 1(a) when  $l_b/D = 5$ .

|               | $\alpha=0.3$ | 0.4   | 0.5   | 0.6   | 0.7   | 0.8   | 0.9   | 0.99  |
|---------------|--------------|-------|-------|-------|-------|-------|-------|-------|
| $\beta = 0.4$ |              |       |       |       |       | 0.485 | 0.338 | 0.202 |
| $\beta = 0.3$ |              | 0.490 | 0.428 | 0.367 | 0.304 | 0.237 | 0.170 |       |
| $\beta = 0.2$ |              |       | 0.357 | 0.321 | 0.284 | 0.243 | 0.198 | 0.153 |
| $\beta = 0.1$ |              | 0.316 | 0.293 | 0.267 | 0.240 | 0.209 | 0.175 | 0.141 |

Table 2.  $F_{\sigma,\lambda_2}$  in Figure 1(a) when  $l_b/D = 5$ .

|               | $\alpha=0.3$ | 0.4   | 0.5   | 0.6   | 0.7   | 0.8    | 0.9    | 0.99    |
|---------------|--------------|-------|-------|-------|-------|--------|--------|---------|
| $\beta = 0.4$ |              |       |       |       |       | 0.361  | 0.179  | —       |
| $\beta = 0.3$ |              |       | 0.397 | 0.325 | 0.248 | 0.166  | 0.0861 | 0.0101  |
| $\beta = 0.2$ |              |       |       | 0.251 | 0.206 | 0.159  | 0.108  | 0.0559  |
| $\beta = 0.1$ |              | 0.211 | 0.182 | 0.150 | 0.117 | 0.0801 | 0.0415 | 0.00354 |

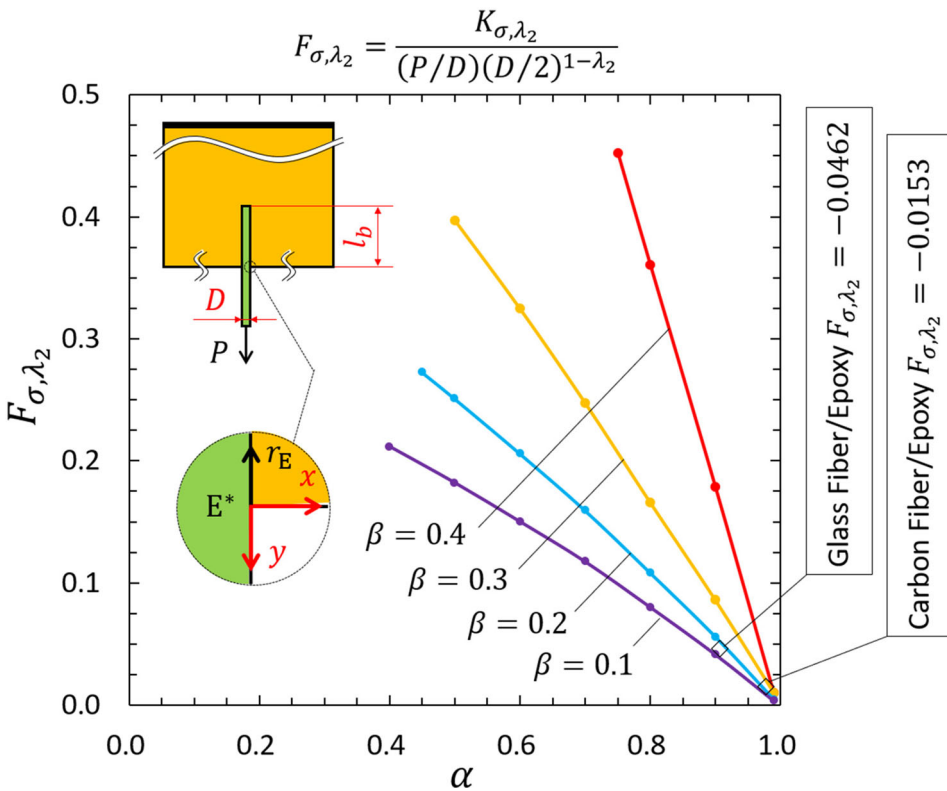


Figure 4.  $F_{\sigma,\lambda_2}$  at the fiber entry point  $E^*$  in pull-out test in Figure 1(a) when  $l_b/D = 5$ .

**Table 3.**  $\lambda_1$  in Figure 3.

|               | $\alpha=0.3$ | 0.4    | 0.5    | 0.6    | 0.7    | 0.8    | 0.9    | 0.99   |
|---------------|--------------|--------|--------|--------|--------|--------|--------|--------|
| $\beta = 0.4$ |              |        |        |        |        | 0.7949 | 0.8001 | 0.8065 |
| $\beta = 0.3$ |              |        | 0.6904 | 0.6951 | 0.7005 | 0.7066 | 0.7133 | 0.7198 |
| $\beta = 0.2$ |              |        | 0.6340 | 0.6396 | 0.6455 | 0.6516 | 0.6580 | 0.6639 |
| $\beta = 0.1$ |              | 0.5908 | 0.5961 | 0.6015 | 0.6071 | 0.6128 | 0.6187 | 0.6241 |

**Table 4.**  $\lambda_2$  in Figure 4.

|               | $\alpha=0.3$ | 0.4    | 0.5    | 0.6    | 0.7    | 0.8    | 0.9    | 0.99  |
|---------------|--------------|--------|--------|--------|--------|--------|--------|-------|
| $\beta = 0.4$ |              |        |        |        |        | 0.9886 | 0.9973 | 1.000 |
| $\beta = 0.3$ |              |        | 0.9585 | 0.9748 | 0.9866 | 0.9944 | 0.9987 | 1.000 |
| $\beta = 0.2$ |              |        | 0.9722 | 0.9832 | 0.9911 | 0.9962 | 0.9991 | 1.000 |
| $\beta = 0.1$ |              | 0.9680 | 0.9791 | 0.9874 | 0.9933 | 0.9972 | 0.9993 | 1.000 |

**Table 5.**  $F_{\sigma, \lambda_1}$  values from Table 1 and Figure 3 by using interpolation.

| $\alpha$                | 0.9775 |        |        |        |
|-------------------------|--------|--------|--------|--------|
| $F_{\sigma, \lambda_1}$ | 0.1459 | 0.1601 | 0.1804 | 0.2214 |
| $\beta$                 | 0.1    | 0.2    | 0.3    | 0.4    |

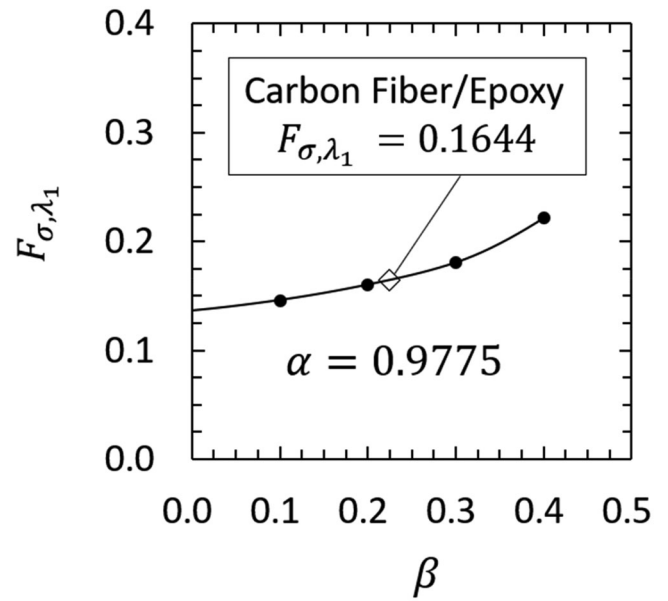
Figure 4 and Table 2 illustrate the normalized ISSF  $F_{\sigma, \lambda_2}$  by varying  $\alpha$ ,  $\beta$ . The value of singular index  $\lambda_2$  is shown in Table 4. A material combination for Carbon fiber/Epoxy ( $\lambda_2 = 0.9999$ ) can be plotted in Figure 4 as  $F_{\sigma, \lambda_2} = 0.0153$ . Then, when  $D = 20\mu\text{m}$ ,  $l_b = 100\mu\text{m}$ , and  $P = 1\text{MPa} \cdot 20\mu\text{m} \cdot 1\text{mm} = 0.02\text{N}$ , we have  $K_{\sigma, \lambda_2} = -0.0153\text{MPa} \cdot \text{m}^{1-0.9999}$ . Another material combination for Glass fiber/Epoxy ( $\lambda_2 = 0.9992$ ),  $F_{\sigma, \lambda_2} = 0.0462$  can be plotted in Figure 4. Then, when  $D = 20\mu\text{m}$ ,  $l_b = 100\mu\text{m}$  and  $P = 1\text{MPa} \cdot 20\mu\text{m} \cdot 1\text{mm} = 0.02\text{N}$ , we have  $K_{\sigma, \lambda_2} = -0.0463\text{MPa} \cdot \text{m}^{1-0.9992}$ .

It can be seen that the normalized ISSFs  $F_{\sigma, \lambda_1}$  and  $F_{\sigma, \lambda_2}$  at the fiber entry point in fiber pull-out problem have smaller values when  $\beta$  is smaller. The normalized ISSFs  $F_{\sigma, \lambda_1}$  and  $F_{\sigma, \lambda_2}$  at the fiber entry point in fiber pull-out problem have smaller values when  $\alpha$  is larger. However, singular index  $\lambda_1$  is larger when  $\beta$  is larger whereas  $\lambda_2$  is larger when  $\beta$  is smaller. Singular indexes  $\lambda_1$  and  $\lambda_2$  are larger when  $\alpha$  is larger.

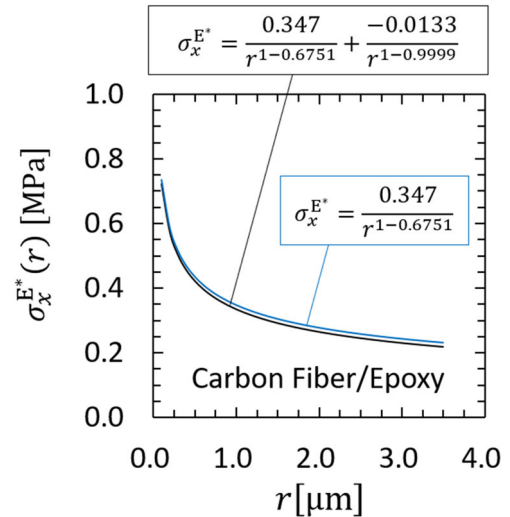
From Eq. (1), the debonding stress  $\sigma_x^i$  becomes larger when the ISSFs  $K_{\sigma, \lambda_1}$ ,  $K_{\sigma, \lambda_2}$  are larger or the singular indexes  $\lambda_1$  and  $\lambda_2$  are smaller. The ISSF  $F_{\sigma, \lambda_1} = 0.164$  of Carbon fiber/Epoxy is smaller than the ISSF  $F_{\sigma, \lambda_1} = 0.198$  of Glass fiber/Epoxy. And  $\lambda_1 = 0.6751$  of Carbon fiber/Epoxy is larger than  $\lambda_1 = 0.6592$  of Glass fiber/Epoxy. Since both  $\lambda_2$  values are very close to 1,  $F_{\sigma, \lambda_1}$  and  $\lambda_1$  mainly controls the interface debonding stress. Therefore, the debonding singular stress  $\sigma_x^i$  of Carbon fiber/Epoxy is smaller than the debonding singular stress  $\sigma_x^i$  of Glass fiber/Epoxy.

#### 4. How to calculate the ISSF from the reference solution

In this section, how to use the reference solution in Figures 3, 4 and Tables 1 and 2 is explained for specific material combination, for example, Carbon fiber/Epoxy and Glass fiber/Epoxy. Figures 3, 4 and Tables 1 and 2 show the normalized ISSF  $F_{\sigma, \lambda_1}$  and  $F_{\sigma, \lambda_2}$  in Figure 1(a) when  $l_b/D = 5$ .

**Figure 5.**  $F_{\sigma, \lambda_1}$  values when  $\alpha = 0.9775$ .**Table 6.** Comparison of ISSFs from interpolation and RWCIM.

| Material combination   | RWCIM   | interpolation | Difference |
|--|---------|---------------|------------|
| $\alpha = 0.9775$ $\lambda_1 = 0.6751$ $F_{\sigma, \lambda_1}$ | 0.1637  | 0.1644        | 1%         |
| $\beta = 0.2250$ $\lambda_2 = 0.9999$ $F_{\sigma, \lambda_2}$  | 0.01531 | 0.01330       | -13%       |
| $\alpha = 0.9071$ $\lambda_1 = 0.6592$ $F_{\sigma, \lambda_1}$ | 0.1976  | 0.1946        | -1%        |
| $\beta = 0.2016$ $\lambda_2 = 0.9992$ $F_{\sigma, \lambda_2}$  | 0.04616 | 0.05150       | 12%        |

**Figure 6.** Stress distribution with and without the second term.

From Figures 3, 4 and Tables 1 and 2, values of  $F_{\sigma, \lambda_1}$  and  $F_{\sigma, \lambda_2}$  can be interpolated in the following way.

For carbon fiber/epoxy, we have  $E_F = 276\text{GPa}$   $\nu_F = 0.30$   $E_M = 3.03$   $\nu_M = 0.35$ . From Eq. (3), Dundurs parameters are  $\alpha = 0.9775$  and  $\beta = 0.2250$ . Also, from Eq. (2), we have the singular indexes  $\lambda_1 = 0.6751$  and  $\lambda_2 = 0.9999$ .

First, from Table 1 and Figure 3, the normalized ISSF value  $F_{\sigma, \lambda_1}$  under  $\alpha = 0.9775$  can be interpolated as shown in Table 5 when  $\beta = 0.1, 0.2, 0.3, 0.4$ . Then, the results are indicated in Figure 5 and Table 5.



Next, as shown in Table 5,  $F_{\sigma, \lambda_1}$  value can be interpolated when  $\beta = 0.2250$  under  $\alpha = 0.9775$ . The interpolated value of  $F_{\sigma, \lambda_1} = 0.1644$  is in good agreement with the RWCIM  $F_{\sigma, \lambda_1} = 0.1637$ . The difference is within 1%. Then, the ISSF value  $K_{\sigma, \lambda_1} = 0.347 \text{MPa} \cdot \text{m}^{1-0.6751}$  can be calculated by using Eq. (6). Similarly,  $F_{\sigma, \lambda_2}$  value of carbon fiber/epoxy can be interpolated from Table 2 and Figure 4, as shown in Table 6.

For glass fiber/epoxy, we have  $E_F = 75 \text{GPa}$   $\nu_F = 0.17$   $E_M = 3.3$   $\nu_M = 0.35$ . Then, from Eq. (3), Dundurs parameters are  $\alpha = 0.9071$ ,  $\beta = 0.2016$ . From Eq. (2), singular indexes  $\lambda_1 = 0.6592$ ,  $\lambda_2 = 0.9992$  can be obtained. Then, in a similar way,  $F_{\sigma, \lambda_1}$ ,  $F_{\sigma, \lambda_2}$  of glass fiber/epoxy can be

interpolated. Table 6 indicates the interpolated  $F_{\sigma, \lambda_1}$ ,  $F_{\sigma, \lambda_2}$  in comparison with the analytical results obtained by RWCIM.

As shown in Table 6, it is seen that  $F_{\sigma, \lambda_1}$  values can be interpolated within 1% error although  $F_{\sigma, \lambda_2}$  values are interpolated within 20% error. This large 20% difference of  $F_{\sigma, \lambda_2}$  is due to almost no singularity as  $\lambda_2 = 0.9999 \cong 1$  and  $\lambda_2 = 0.9992 \cong 1$ . If this second term singularity in Eq.(1) is significant, for example, when  $\lambda_2 = 0.85$ , the difference of  $F_{\sigma, \lambda_2}$  can be very small and within 1%.

It should be noted that since  $\lambda_2 \cong 1$ , the stress distribution along the interface is not affected by the  $F_{\sigma, \lambda_2}$  difference. For example, Figure 6 shows the stress distribution with and without the second term  $F_{\sigma, \lambda_2}$  for  $\alpha = 0.9775$  and  $\beta = 0.2250$ . The stress value when  $r = 0.5 \mu\text{m}$  is  $0.4218 \text{MPa}$  when  $F_{\sigma, \lambda_2}$  is considered, and is  $0.4351 \text{MPa}$  when  $F_{\sigma, \lambda_2}$  is not considered. Since the second term in Eq. (1) contributes only 3%, the ISSF difference of  $F_{\sigma, \lambda_2}$  by 20% affects only  $3\% \times 20\% = 0.6\%$ .

Figure 7 compares the stress distribution of ISSF obtained by interpolation and RWCIM. The difference of stress distribution obtained by the two method is about 1%, and is mainly caused by the  $F_{\sigma, \lambda_1}$  difference. The singular stress distributions coincide with each other within 1% difference in the range  $r \leq 4 \mu\text{m}$  between the interpolation and RWCIM even though the difference of the  $F_{\sigma, \lambda_2}$  is 13%.

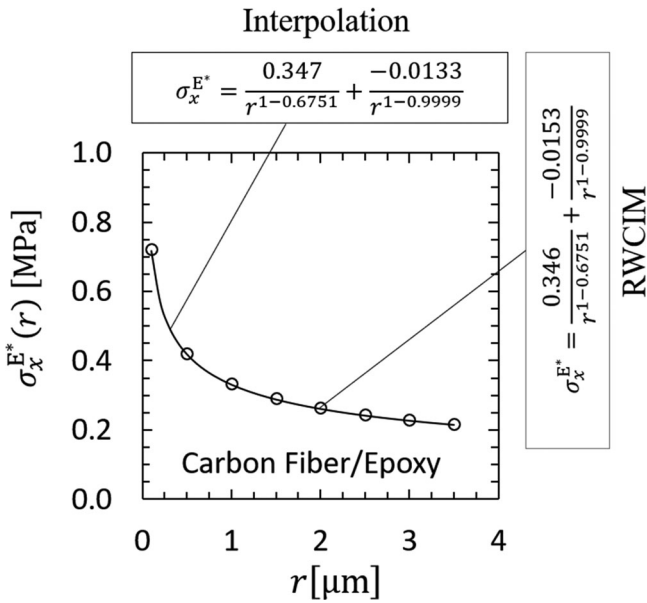


Figure 7. Stress distribution with ISSF from interpolation and RWCIM.

## 5. Effect of material combination: ISSF ratio of pull-out test to micro-bond test

In the previous study [27], the ISSF at Point E\* in pull-out test in Figure 1(a) is compared with the ISSF at Point E in micro-bond test in Figure 1(b). Then, for Glass fiber/epoxy, it was found that the ISSF ratio  $K_{\sigma}^{E^*} / K_{\sigma}^E \cong 0.75$

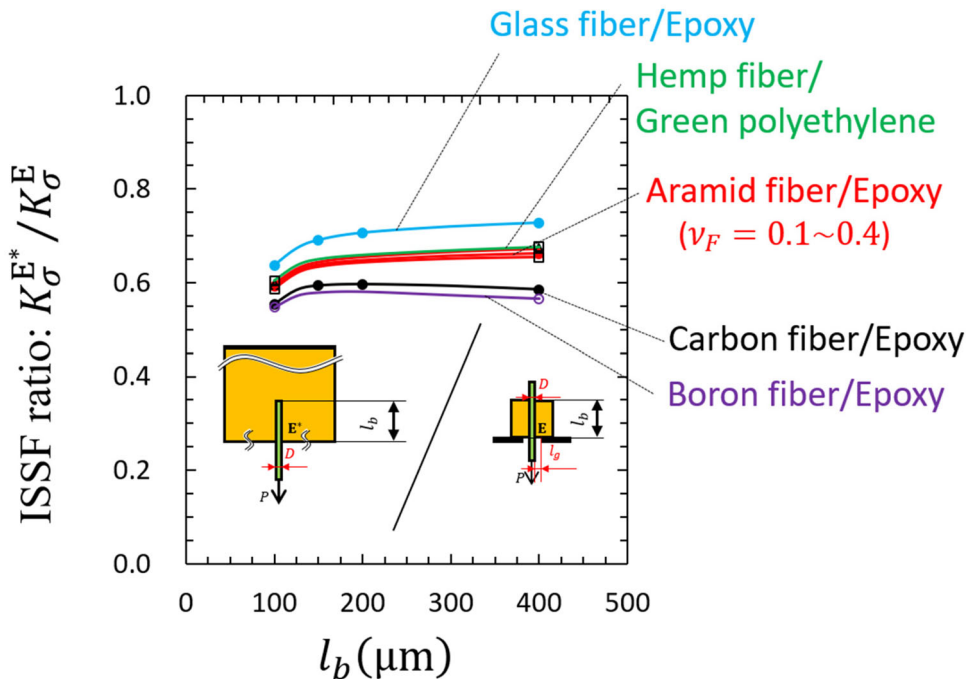


Figure 8. ISSF ratio  $K_{\sigma}^{E^*} / K_{\sigma}^E$  of pull-out test and microbond test when  $l_g = 20 \mu\text{m}$ .

**Table 7.** ISSF ratio  $K_{\sigma}^{E^*}/K_{\sigma}^E$  of pull-out test and microbond test when  $l_b = 20\mu\text{m}$ .

| $l_b[\mu\text{m}]$ | 100   | 150   | 200   | 400   | $E_F[\text{GPa}]$ | $\nu_F$ | $E_M[\text{GPa}]$ | $\nu_F$ |
|--------------------|-------|-------|-------|-------|-------------------|---------|-------------------|---------|
| Glass              | 0.637 | 0.691 | 0.707 | 0.728 | 75                | 0.17    | 3.3               | 0.35    |
| Hemp               | 0.604 | —     | —     | 0.677 | 7.37              | 0.3     | 0.258             | 0.3     |
| Aramid             | 0.597 | —     | —     | 0.673 | 130               | 0.1     | 3.3               | 0.35    |
| Aramid             | 0.592 | —     | —     | 0.662 | 130               | 0.3     | 3.3               | 0.35    |
| Aramid             | 0.587 | —     | —     | 0.654 | 130               | 0.4     | 3.3               | 0.35    |
| Carbon             | 0.554 | 0.593 | 0.596 | 0.585 | 276               | 0.3     | 3.03              | 0.35    |
| Boron              | 0.547 | —     | —     | 0.566 | 400               | 0.3     | 3.3               | 0.35    |

independent of the dimension  $l_b$ . In other words, the ISSF at Point E in micro-bond test is about 1.5 times of that at Point E\* in pull-out test. This conclusion is useful since the micro-bond test is more convenient than the pull-out test reflecting real composites. In this study, therefore, this ISSF ratio is investigated by varying Fiber/Resin combination.

Figure 8 and Table 7 show the results for Hemp fiber/Green polyethylene, Aramid fiber/Epoxy, Carbon fiber/Epoxy and Boron fiber/Epoxy. It is seen that the ISSF ratio  $K_{\sigma}^{E^*}/K_{\sigma}^E$  is almost constant independent of  $l_b$  in the range  $K_{\sigma}^{E^*}/K_{\sigma}^E \cong 0.55 \sim 0.75$ . To investigate the effect of fiber Poisson's ratio  $\nu_F$ , the ISSF ratio  $K_{\sigma}^{E^*}/K_{\sigma}^E$  of Aramid fiber/Epoxy is indicated by varying  $\nu_F = 0.1, 0.3, 0.4$ . When  $\nu_F = 0.1$ , the ratio  $K_{\sigma}^{E^*}/K_{\sigma}^E = 0.673$  is a bit larger and when  $\nu_F = 0.4$ ,  $K_{\sigma}^{E^*}/K_{\sigma}^E = 0.654$  is a bit smaller compared to  $K_{\sigma}^{E^*}/K_{\sigma}^E = 0.662$  when  $\nu_F = 0.3$ . As a conclusion, the effect of  $\nu_F$  on the ratio  $K_{\sigma}^{E^*}/K_{\sigma}^E$  is not very large. The ISSF of pull-out test can be roughly estimated from the ISSF of micro-bond test. In this section, the difference between pull-out test and microbond test is expressed as the ISSF ratio. The validity of the ISSF ratios is discussed in Appendix C for the experiment of adhesive lap joints in Figure 1(c).

## 6. Conclusions

Recent studies showed the ISSF is useful for evaluating the bonded strength. In this paper, ISSF solution at the fiber entry point was indicated under arbitrary material combination for the single-fiber subjected to pull-out force. This reference solution can be used for analyzing various kinds of fibers and various aspect ratios of the fiber coupled with the proportional method. The proportional method can be used conveniently since only the FEM stress at the interface corner is focused by applying a similar mesh to the unknown and the reference problem.

## Declaration of interests

The authors declare that they have no known competing financial interests or personal relationships that could have appeared to influence the work reported in this paper.

## ORCID

Dong Chen  <http://orcid.org/0000-0001-8354-262X>

## Reference

- [1] Q. Wu, M. Li, Y. Gu, Y. Li, and Z. Zhang, Nano-analysis on the structure and chemical composition of the interphase region in carbon fiber composite, *Compos. Part A: Appl. Sci. Manuf.*, vol. 56, pp. 143–149, 2014. DOI: [10.1016/j.compositesa.2013.10.003](https://doi.org/10.1016/j.compositesa.2013.10.003).
- [2] F. Teklal, A. Djebbar, S. Allaoui, G. Hivet, Y. Joliff, and B. Kacimi, A review of analytical models to describe pull-out behavior – fiber/matrix adhesion, *Compos. Struct.*, vol. 201, pp. 791–815, 2018. DOI: [10.1016/j.compstruct.2018.06.091](https://doi.org/10.1016/j.compstruct.2018.06.091).
- [3] M. L. Williams, The stresses around a fault or crack in dissimilar media, *Bull. Seismol. Soc. Am.*, vol. 49, pp. 199–204, 1959.
- [4] J. R. Rice, Elastic fracture mechanics concepts for interfacial cracks, *J. Appl. Mech. Trans. ASME.*, vol. 55, no. 1, pp. 98–103, 1988. DOI: [10.1115/1.3173668](https://doi.org/10.1115/1.3173668).
- [5] J. W. Hutchinson, M. E. Mear, and J. R. Rice, Crack paralleling an interface between dissimilar materials, *J. Appl. Mech. Trans. ASME.*, vol. 54, no. 4, pp. 828–832, 1987. DOI: [10.1115/1.3173124](https://doi.org/10.1115/1.3173124).
- [6] R. J. Scheer, and J. A. Nairn, A comparison of several fracture mechanics methods for measuring interfacial toughness with microbond tests, *J Adhes.*, vol. 53, no. 1-2, pp. 45–68, 1995. DOI: [10.1080/00218469508014371](https://doi.org/10.1080/00218469508014371).
- [7] E. Pisanova, S. Zhandarov, E. Mäder, I. Ahmad, and R. J. Young, Three techniques of interfacial bond strength estimation from direct observation of crack initiation and propagation in polymer-fibre systems, *Compos. Part A: Appl. Sci. Manuf.*, vol. 32, no. 3/4, pp. 435–443, 2001. DOI: [10.1016/S1359-835X\(00\)00054-3](https://doi.org/10.1016/S1359-835X(00)00054-3).
- [8] C. Marotzke, and L. Qiao, Interfacial crack propagation arising in single-fiber pull-out tests, *Compos. Sci. Technol.*, vol. 57, no. 8, pp. 887–897, 1997. DOI: [10.1016/S0266-3538\(96\)00179-0](https://doi.org/10.1016/S0266-3538(96)00179-0).
- [9] N.-A. Noda, T. Miyazaki, T. Uchikoba, R. Li, Y. Sano, and Y. Takase, Convenient debonding strength evaluation based on the intensity of singular stress for adhesive joints, *J. Japan Instit. Electron. Packag.*, vol. 17, no. 2, pp. 132–142, 2014. DOI: [10.5104/jiep.17.132](https://doi.org/10.5104/jiep.17.132).
- [10] Y. Suzuki, Adhesive tensile strength of scarf and butt joints of steel plates (Relation between adhesive layer thicknesses and adhesive strengths of joints), *JSME Int. J.*, vol. 30, no. 265, pp. 1042–1051, 1987. DOI: [10.1299/jsme1987.30.1042](https://doi.org/10.1299/jsme1987.30.1042).
- [11] N.-A. Noda, T. Miyazaki, R. Li, T. Uchikoba, Y. Sano, and Y. Takase, Debonding strength evaluation in terms of the intensity of singular stress at the interface corner with and without fictitious crack, *Int. J. Adhes. Adhes.*, vol. 61, pp. 46–64, 2015. DOI: [10.1016/j.ijadhadh.2015.04.005](https://doi.org/10.1016/j.ijadhadh.2015.04.005).
- [12] T. Miyazaki, N.-A. Noda, F. Ren, Z. Wang, Y. Sano, and K. Iida, Analysis of intensity of singular stress field for bonded cylinder and bonded pipe in comparison with bonded plate, *Int. J. Adhes. Adhes.*, vol. 77, pp. 118–137, 2017. DOI: [10.1016/j.ijadhadh.2017.03.019](https://doi.org/10.1016/j.ijadhadh.2017.03.019).
- [13] N.-A. Noda, F. Ren, R. Takaki, Z. Wang, K. Oda, T. Miyazaki, and Y. Sano, Intensity of singular stress field over the entire bond line thickness range useful for evaluating the adhesive strength for plate and cylinder butt joints, *Int. J. Adhes. Adhes.*, vol. 85, pp. 234–250, 2018. DOI: [10.1016/j.ijadhadh.2018.05.013](https://doi.org/10.1016/j.ijadhadh.2018.05.013).
- [14] T. Miyazaki, N.-A. Noda, Z. Wang, and Y. Sano, Analysis of intensity of singular stress field for bonded cylinder in comparison with bonded plate, *Trans. JSME (in Japanese)*, vol. 81, no. 829, pp. 15-00210–15-00210, 2015. DOI: [10.1299/transjsme.15-00210](https://doi.org/10.1299/transjsme.15-00210).
- [15] N.-A. Noda, F. Ren, R. Takaki, K. Tsuboi, Y. Sano, Y. Takase, and T. Miyazaki, Validity of the adhesive strength evaluation method based on the intensity of singular stress field in two-dimensional modelling, *J. Japan Instit. Electron. Packag.*, vol. 21, no. 4, pp. 299–310, 2018. DOI: [10.5104/jiep.21.299](https://doi.org/10.5104/jiep.21.299).
- [16] K. Oda, K. Kamisugi, and N. A. Noda, Analysis of stress intensity factor for interface cracks based on proportional method,



- JSMET, vol. 75, no. 752, pp. 476–482, 2009. DOI: [10.1299/kikaia.75.476](https://doi.org/10.1299/kikaia.75.476).
- [17] H. Nisitani, and T. Teranishi, Highly accurate values of KI and KII of axially symmetrical cracked body subjected to tension obtained by FEM, *Struct. Mater.*, vol. 6, pp. 461–469, 2000.
- [18] H. Nisitani, and T. Teranishi, KI of a circumferential crack emanating from an ellipsoidal cavity obtained by the crack tip stress method in FEM, *Eng. Fract. Mech.*, vol. 71, no. 4-6, pp. 579–585, 2004. DOI: [10.1016/S0013-7944\(03\)00035-3](https://doi.org/10.1016/S0013-7944(03)00035-3).
- [19] T. Miyazaki, N.-A. Noda, T. Uchikoba, R. Li, and Y. Sano, Proposal of a convenient and accurate method for evaluation of debonding strength, *Trans. Soc. Automot. Eng. Japan.*, vol. 45, no. 5, pp. 895–901, 2014. DOI: [10.11351/jsaeronbun.45.895](https://doi.org/10.11351/jsaeronbun.45.895).
- [20] T. Miyazaki, N.-A. Noda, and Y. Sano, A precise and efficient analytical method to obtain two distinct intensities of singular stress fields for single lap joint, *J. Japan Instit. Electron. Packag.*, vol. 21, no. 2, pp. 166–177, 2018. DOI: [10.5104/jiep.21.166](https://doi.org/10.5104/jiep.21.166).
- [21] T. Miyazaki, and N.-A. Noda, Evaluation of debonding strength of single lap joint by the intensity of singular stress field, *J. Phys. Conf. Ser.*, vol. 842, pp. 012078, 2017. DOI: [10.1088/1742-6596/842/1/012078](https://doi.org/10.1088/1742-6596/842/1/012078).
- [22] D.-H. Chen, and H. Nisitani, Singular stress field near the corner of jointed dissimilar materials, *J. Appl. Mech. Trans. ASME.*, vol. 60, no. 3, pp. 607–613, 1993. DOI: [10.1115/1.2900847](https://doi.org/10.1115/1.2900847).
- [23] D.-H. Chen, and H. Nisitani, Singular stress field in two bonded wedges, *JSMET*, vol. 58, no. 547, pp. 457–464, 1992. DOI: [10.1299/kikaia.58.457](https://doi.org/10.1299/kikaia.58.457).
- [24] N.-A. Noda, R. Li, T. Miyazaki, R. Takaki, and Y. Sano, Convenient adhesive strength evaluation method in terms of the intensity of singular stress field, *Int. J. Comput. Methods.*, vol. 16, no. 01, pp. 1850085, 2019. DOI: [10.1142/S0219876218500858](https://doi.org/10.1142/S0219876218500858).
- [25] S. Zhandarov, and E. Mäder, Characterization of fiber/matrix interface strength: Applicability of different tests, approaches and parameters, *Compos. Sci. Technol.*, vol. 65, no. 1, pp. 149–160, 2005. DOI: [10.1016/j.compscitech.2004.07.003](https://doi.org/10.1016/j.compscitech.2004.07.003).
- [26] N.-A. Noda, D. Chen, G. Zhang, and Y. Sano, Single-fiber pull-out analysis comparing the intensities of singular stress fields (ISSFs) at fiber end/entry points, *Int. J. Mech. Sci.*, vol. 165, pp. 105196, 2020. DOI: [10.1016/j.ijmecsci.2019.105196](https://doi.org/10.1016/j.ijmecsci.2019.105196).
- [27] D. Chen, N.-A. Noda, R. Takaki, and Y. Sano, Intensity of singular stress fields (ISSFs) in micro-bond test in comparison with ISSFs in pull-out test, *Int. J. Mech. Sci.*, vol. 183, pp. 105817, 2020. DOI: [10.1016/j.ijmecsci.2020.105817](https://doi.org/10.1016/j.ijmecsci.2020.105817).
- [28] E. D. Reedy, Jr., and T. R. Guess, Comparison of butt tensile strength data with interface corner stress intensity factor prediction, *Int. J. Solids Struct.*, vol. 30, no. 21, pp. 2929–2936, 1993. DOI: [10.1016/0020-7683\(93\)90204-K](https://doi.org/10.1016/0020-7683(93)90204-K).
- [29] Z. Qian, and A. R. Akisanya, An Experimental investigation of failure initiation in bonded joints, *Acta Mater.*, vol. 46, no. 14, pp. 4895–4904, 1998. DOI: [10.1016/S1359-6454\(98\)00200-6](https://doi.org/10.1016/S1359-6454(98)00200-6).
- [30] A. Mintzas, and D. Nowell, Validation of an Hcr-based fracture initiation criterion for adhesively bonded joints, *Eng. Fract. Mech.*, vol. 80, pp. 13–27, 2012. DOI: [10.1016/j.engfracmech.2011.09.020](https://doi.org/10.1016/j.engfracmech.2011.09.020).
- [31] P. E. W. Labossiere, M. L. Dunn, and S. J. Cunningham, Application of bimaterial interface corner failure mechanics to silicon/glass anodic bonds, *J. Mech. Phys. Solids.*, vol. 50, no. 3, pp. 405–433, 2002. DOI: [10.1016/S0022-5096\(01\)00087-4](https://doi.org/10.1016/S0022-5096(01)00087-4).
- [32] D. B. Bogy, Edge-bonded dissimilar orthogonal elastic wedges under normal and shear loading, *J. Appl. Mech. Trans. ASME*, vol. 35, no. 3, pp. 460–466, 1968. DOI: [10.1115/1.3601236](https://doi.org/10.1115/1.3601236).
- [33] D. B. Bogy, Two edge-bonded elastic wedges of different materials and wedge angles under surface tractions, *J. Appl. Mech. Trans. ASME*, vol. 38, no. 2, pp. 377–386, 1971. DOI: [10.1115/1.3408786](https://doi.org/10.1115/1.3408786).
- [34] W. C. Carpenter, Mode I and mode II stress intensities for plates with cracks of finite opening, *Int. J. Fract.*, vol. 26, no. 3, pp. 201–214, 1984. DOI: [10.1007/BF01140628](https://doi.org/10.1007/BF01140628).
- [35] J. Dundurs, Effect of elastic constants on stress in a composite under plane deformation, *J. Compos. Mater.*, vol. 1, no. 3, pp. 310–322, 1967. DOI: [10.1177/002199836700100306](https://doi.org/10.1177/002199836700100306).
- [36] T. Suga, G. Ellsner, and S. Schmauder, Composite parameters and mechanical compatibility of material joints, *J. Compos. Mater.*, vol. 22, no. 10, pp. 917–934, 1988. DOI: [10.1177/002199838802201002](https://doi.org/10.1177/002199838802201002).
- [37] R. Yuuki, *Mechanics of interface*, Baifukan, Tokyo, 1993.
- [38] N.-A. Noda, X. Chen, Y. Sano, MA Wahab, H. Maruyama, R. Fujisawa, and Y. Takase, Effect of pitch difference between the bolt-nut connections upon the anti-loosening performance and fatigue life, *Mater. Des.*, vol. 96, pp. 476–489, 2016. DOI: [10.1016/j.matdes.2016.01.128](https://doi.org/10.1016/j.matdes.2016.01.128).
- [39] N.-A. Noda, R. Takaki, Y. Shen, A. Inoue, Y. Sano, D. Akagi, Y. Takase, and P. Galvez, Strain rate concentration factor for flat notched specimen to predict impact strength for polymeric materials, *Mech. Mater.*, vol. 131, pp. 141–157, 2019. DOI: [10.1016/j.mechmat.2019.01.011](https://doi.org/10.1016/j.mechmat.2019.01.011).
- [40] Z. Wang, N.-A. Noda, M. Ueno, and Y. Sano, Optimum Design of Ceramic Spray Coating Evaluated in Terms of Intensity of Singular Stress Field, *Steel Research Int.*, vol. 88, no. 7, pp. 1600353, 2017. DOI: [10.1002/srin.201600353](https://doi.org/10.1002/srin.201600353).
- [41] M. Stern and M. L. Soni, On the computation of stress intensities at fixed-free corners, *Int. J. Solids Struct.*, vol. 12, no. 5, pp. 331–337, 1976. [https://doi.org/10.1016/0020-7683\(76\)90023-8](https://doi.org/10.1016/0020-7683(76)90023-8). DOI: [10.1016/0020-7683\(76\)90023-8](https://doi.org/10.1016/0020-7683(76)90023-8).
- [42] C. Atkinson, J. Avila, E. Betz, and R. E. Smelser, The rod pull out problem, theory and experiment, *J. Mech. Phys. Solids.*, vol. 30, no. 3, pp. 97–120, 1982. DOI: [10.1016/0022-5096\(82\)90019-9](https://doi.org/10.1016/0022-5096(82)90019-9).
- [43] G. L. Povirk, and A. Needleman, Finite element simulations of fiber pull-out, *J. Eng. Mater. Technol. Trans. ASME.*, vol. 115, no. 3, pp. 286–291, 1993. DOI: [10.1115/1.2904220](https://doi.org/10.1115/1.2904220).
- [44] L. B. Freund, Axial force needed to slide a circular fiber along a hole in an elastic material and implications for fiber pull-out, *Eur. J. Mech. A/Solids.*, vol. 11, pp. 1–19, 1992.
- [45] X. Zhang, H.-Y. Liu, and Y.-W. Mai, Effects of fibre debonding and sliding on the fracture behaviour of fibre-reinforced composites, *Compos. Part A: Appl. Sci. Manuf.*, vol. 35, no. 11, pp. 1313–1323, 2004. DOI: [10.1016/j.compositesa.2004.03.011](https://doi.org/10.1016/j.compositesa.2004.03.011).
- [46] J. W. Hutchinson, and H. M. Jensen, Models of fiber debonding and pullout in brittle composites with friction, *Mech. Mater.*, vol. 9, no. 2, pp. 139–163, 1990. DOI: [10.1016/0167-6636\(90\)90037-G](https://doi.org/10.1016/0167-6636(90)90037-G).
- [47] W. C. Carpenter, and C. Byers, A path independent integral for computing stress intensities for V-notched cracks in a bi-material, *Int. J. Fract.*, vol. 35, no. 4, pp. 245–268, 1987. DOI: [10.1007/BF00276356](https://doi.org/10.1007/BF00276356).
- [48] G. B. Sinclair, M. Okajima, and J. H. Griffin, Path independent integrals for computing stress intensity factors at sharp notches in elastic plates, *Int. J. Numer. Meth. Eng.*, vol. 20, no. 6, pp. 999–1008, 1984. DOI: [10.1002/nme.1620200603](https://doi.org/10.1002/nme.1620200603).
- [49] M. Stern, E. B. Becker, and R. S. Dunham, A contour integral computation of mixed-mode stress intensity factors, *Int. J. Fract.*, vol. 12, pp. 359–368, 1976. DOI: [10.1007/BF00032831](https://doi.org/10.1007/BF00032831).
- [50] R. Li, N.-A. Noda, R. Takaki, Y. Sano, Y. Takase, and T. Miyazaki, Most suitable evaluation method for adhesive strength to minimize bend effect in lap joints in terms of the intensity of singular stress field, *Int. J. Adhes. Adhes.*, vol. 86, pp. 45–58, 2018. DOI: [10.1016/j.ijadhadh.2018.08.006](https://doi.org/10.1016/j.ijadhadh.2018.08.006).
- [51] T. Miyazaki, N.-A. Noda, R. Li, T. Uchikoba, and Y. Sano, Debonding criterion for single lap joints from the intensity of singular stress field, *J. Japan Instit. Electron. Packaging.*, vol. 16, no. 2, pp. 143–151, 2013. DOI: [10.5104/jiep.16.143](https://doi.org/10.5104/jiep.16.143).
- [52] R. Takaki, N.-A. Noda, Y. Sano, Y. Takase, Y. Suzuki, and C. Chao, Fractographic Identification of Fracture Origin Mainly Controlled by the Intensity of Singular Stress Field (ISSF) in

Prismatic Butt Joint with Corner Fillet, Int. J. Adhes. Adhes., n.d.:in printing. DOI: 10.1016/j.ijadhadh.2021.102810

- [53] J.-H. Park, J.-H. Choi, and J.-H. Kweon, Evaluating the strengths of thick aluminum-to-aluminum joints with different adhesive lengths and thicknesses, Compos. Struct., vol. 92, no. 9, pp. 2226–2235, 2010. DOI: 10.1016/j.compstruct.2009.08.037.

## Appendix A: Reference solution obtained by using reciprocal work contour integral method (RWCIM)

The ISSFs  $K_{\sigma, \lambda_1^E}^E$ ,  $K_{\tau, \lambda_1^E}^E$  at the fiber entry Point E in Figure 1(b) can be calculated by using the proportional method explained in Section 3 from the FEM stress ratios as shown in Eq. (4), which is  $\frac{K_{\sigma, \lambda_1^E}^E}{K_{\sigma, \lambda_1^E}^{E*}} = \frac{\sigma_{FEM, \lambda_1^E}^E}{\sigma_{FEM, \lambda_1^E}^{E*}}$ ,  $\frac{K_{\tau, \lambda_1^E}^E}{K_{\tau, \lambda_1^E}^{E*}} = \frac{\tau_{FEM, \lambda_1^E}^E}{\tau_{FEM, \lambda_1^E}^{E*}}$ . To obtain the reference solution  $K_{\sigma, \lambda_1^E}^{E*}$ ,  $K_{\tau, \lambda_1^E}^{E*}$  the RWCIM may be suitable. This method is based on the concept of Betti's Law, pioneered by Stern et al. [41]. Carpenter et al. [47] and Sinclair et al. [48] adapted this method to the general opening crack problem. By mean of Williams' eigenfunction expansion method, displacement and stress in the vicinity of the interface corner edge can be expressed as [3, 47]:

$$\sigma_{ij} = \sum_{k=1}^{\infty} K_k f_{ij}(\theta, \lambda_k) r^{\lambda_k - 1} \quad (\text{A.1})$$

$$u_i = \sum_{k=1}^{\infty} K_k g_i(\theta, \lambda_k) r^{\lambda_k} \quad (\text{A.2})$$

Here,  $\lambda_k$  is singular index obtained by solving Eq. (2) in Section 3. For most of the material combinations the singular indexes  $\lambda_k^E$  have two real roots  $\lambda_1^E$  and  $\lambda_2^E$  corresponding to two different singular fields [34]. Here,  $K_k$  is ISSF corresponding to singular index  $\lambda_k$ , obtained by RWCIM discussed in this section. As shown in Figure A1, symbol  $r$  is the radial distance away from Point E. Eigenfunctions  $f_{ij}$  and  $g_i$  depend on  $\lambda_k$  and  $\theta$ . When  $\theta = 0$ , and use  $K_{\sigma, \lambda_k}$  to denote  $K_k f_{ij}(\theta, \lambda_k)$ , Eq. (A.1) is expressed as Eq. (1). Denote by  $u_i$  the displacement field and  $\sigma_{ij}$  the traction vector on a contour  $C = C_1 + C_2 + C_3 + C_4 + C_5 + C_6 + C_e$ , as shown in Figure A1, Eq. (A.3) [47] is obtained from Betti's Law:

$$\oint_C (\sigma_{ij} u_i^* - \sigma_{ij}^* u_i) ds = 0 \quad (\text{A.3})$$

Here,  $u_i^*$  and  $\sigma_{ij}^*$  correspond to any other such solution. Contour  $C_e$  is a three-quarter circle contour with a radius  $\varepsilon$ . Separate the contour into  $C_e$  and  $C_R = C_1 + C_2 + C_3 + C_4 + C_5 + C_6$ , Eq. (A.3) becomes [49]:

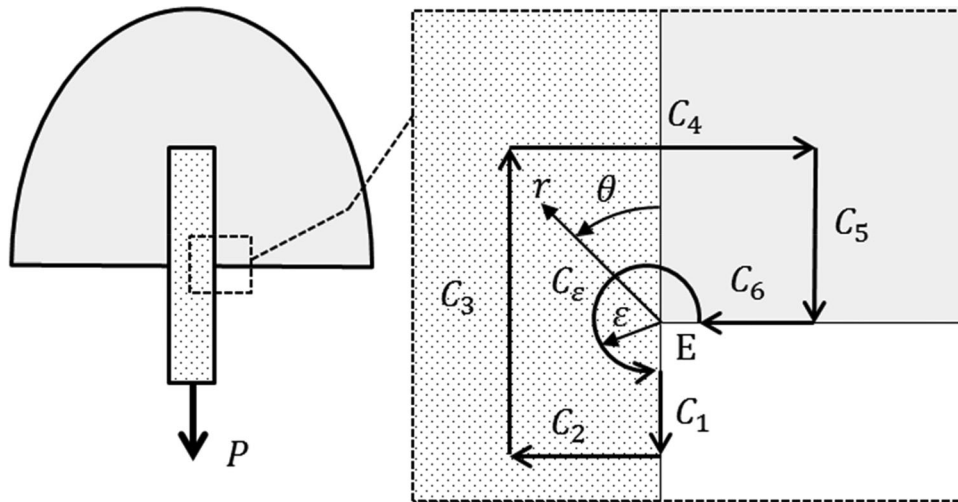


Figure A1. Integral path C for RWCIM ( $C = C_1 + C_2 + C_3 + C_4 + C_5 + C_6$ ).

$$I_e = \int_{C_e} (\sigma_{ij} u_i^* - \sigma_{ij}^* u_i) ds = - \int_{C_R} (\sigma_{ij} u_i^* - \sigma_{ij}^* u_i) ds \quad (\text{A.4})$$

Then, the integral  $I_e$  can be calculated from the path independent contour  $C_R$ , without need for accurate data in the vicinity of the Point E in FEM calculation. ISSF  $K_k$  corresponding to singular index  $\lambda_k$  can then be obtained. Combined with  $f_{ij}$  for  $\sigma$  and  $\tau$  respectively, expressed as  $K_{\sigma, \lambda_1^E}^E$ ,  $K_{\sigma, \lambda_2^E}^E$ ,  $K_{\tau, \lambda_1^E}^E$ ,  $K_{\tau, \lambda_2^E}^E$  in Section 3. Worth mentioning that, for the integral path C shown in Figure A1, contours  $C_1$  and  $C_2$  locate along the stress-free surface, and therefore, the integrals along these contours are zero. The integral path independency can be confirmed as well as the mesh independency [19–21, 24, 26, 27, 50, 51]. Then, RWCIM can be used as the reference solution of the ISSF.

Plane strain condition is selected for carrying out the linear elastic analyses in MSC Marc software. Representation of the selected mesh pattern for developing these analyses is similar to that as shown in Figure 2. Around the interface corner edge eight-node elements are utilized, while for other regions away from the interface corner edge, four-node elements are selected. However, RWCIM requires a large number of calculations for complex operations with matrix as well as numerical integrations along the path. The proportional method may provide the ISSF efficiently as shown in Section 3 from the reference solution. The proportional method coupled with the RWCIM is just as accurate as the RWCIM conveniently and practically especially when calculating the first term by focusing on the FEM stress ratio.

## Appendix B: step-by-step procedure to apply the reference solution coupled with the proportional method to calculate ISSF

Figure B2 illustrates how to calculate the ISSF by applying the reference solution and the proportional method. The flowchart in Figure B1 indicates elementary step-by-step actions.

First of all, as STEP 1, the singularity should be determined, for the 2-dimensional problem of fiber with  $180^\circ$  and matrix with  $90^\circ$  at the singular point. The ISSF in Figures 3 and 4 can be used as reference. For example, this reference is suitable for Point E\* in Figure 1(a), Point A and Point E in Figure 1(b), and Point E\*\* in Figure 1(c). The singular indexes are same for these problems. For the 2-dimensional problem of fiber with  $90^\circ$  and matrix with  $270^\circ$  at the singular point, for example, Point A\* in Figure 1(a). The results of [26] should be used as reference.

As shown in Figure B2, in STEP 2 minimum FEM mesh size  $e_{min}$  are applied to the pull-out problem in Figures 3 and 4 (=reference problem) and the microbond problem of different size (=unknown problem). Stress distribution  $\sigma_{FEM}^*(r)$  obtained from the FEM reference

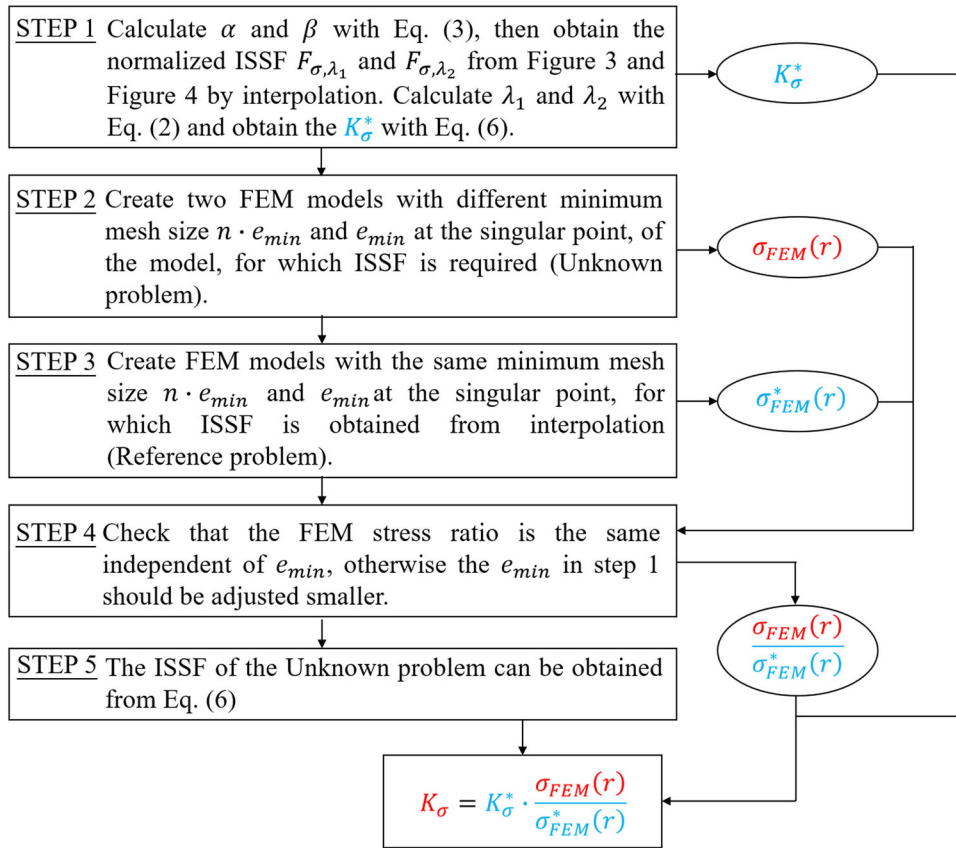


Figure B1. Flow chart of ISSF calculation.

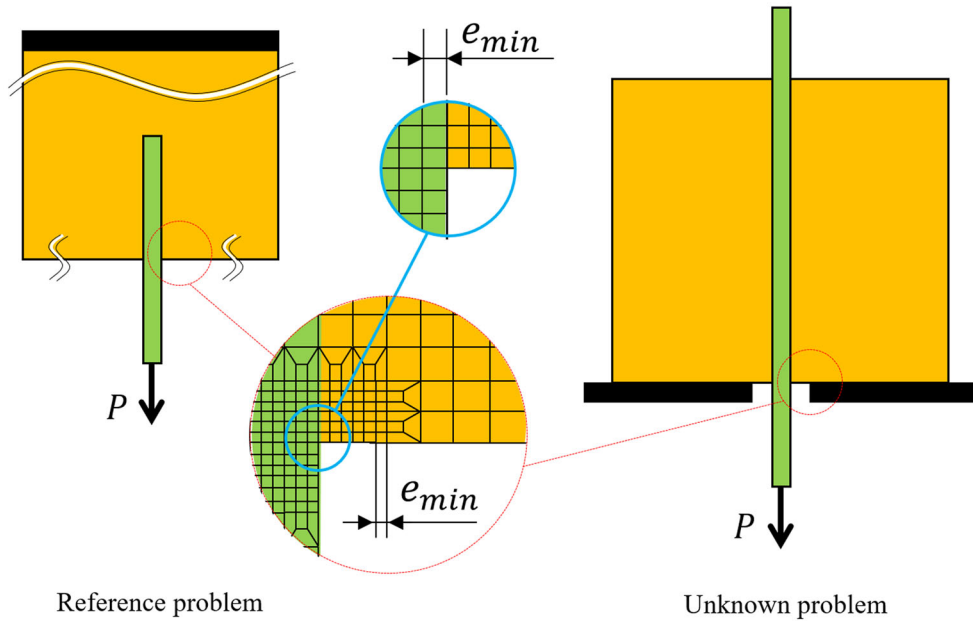
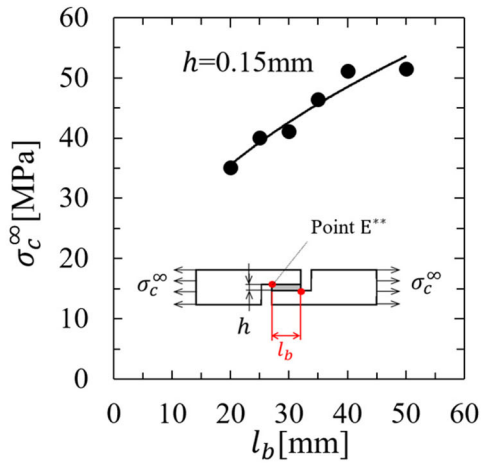


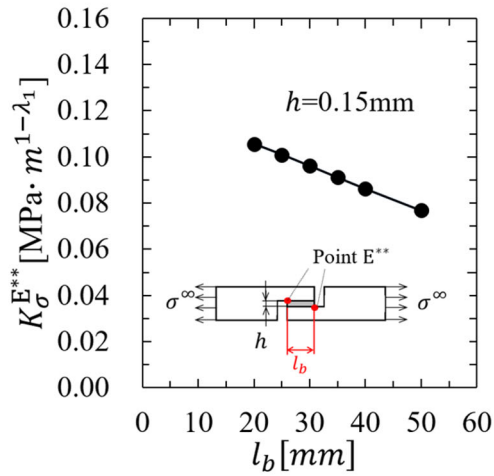
Figure B2. Example of analysis model and mesh pattern.

model and  $\sigma_{FEM}(r)$  obtained from the FEM unknown model can be used to calculate the stress ratio  $\sigma_{FEM}(r) / \sigma_{FEM}^*(r)$  in STEP 3. In STEP 4, this ratio should be same no matter the minimum FEM mesh size is  $e_{min}$  or  $n \cdot e_{min}$ . As the mesh-independency of the stress ratio is investigated, if the  $\sigma_{FEM}(r) / \sigma_{FEM}^*(r)$  of two different  $e_{min}$  are not same, the

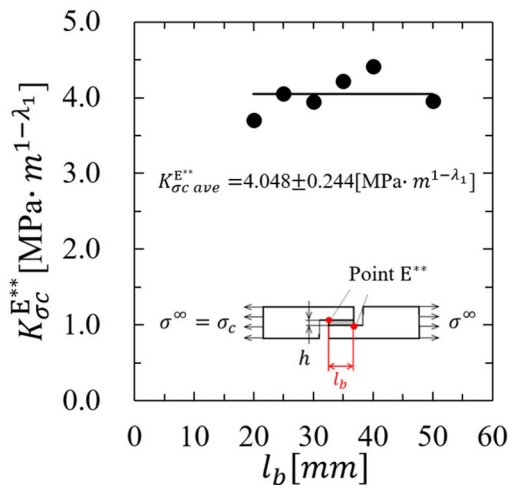
$e_{min}$  in STEP 1 should be adjusted smaller. Since the same FEM mesh is applied around the singular point, the FEM error can be eliminated. STEP 5, the FEM stress ratio can be used as the ISSF ratio. Then, the ISSF of the unknown problem can be provided from the ISSF ratio and the exact ISSF of the reference problem.



**C1(a).** Critical remote tensile stress



**C1 (b).** ISSF  $K_\sigma^B$  under  $\sigma^\infty = 1\text{MPa}$



**C1 (c).** Critical ISSF  $K_{\sigma_c}^{E**}$

## Appendix C: usefulness of ISSF to evaluate adhesive strength

Usually, the single-fiber pull-out test and the microbond test are conducted in terms of the average shear stress without considering the ISSF. In this paper, how to calculate the ISSF is described in detail at the fiber entry point. In this Appendix, the validity of ISSF approach is described in the experiment for the adhesive lap joint whose singular stress field is identical as shown in Figure 1 [19–21, 24, 50, 51]. Another verification can be seen in the experiment for prismatic and cylindrical adhesive butt joints in [9–15, 52, 53].

Figure C1(a) shows the critical debonding stress  $\sigma^\infty = \sigma_c$  for lap joint by varying the bonded length  $l_b$ . In this experiment [53], 6061-T6 aluminum alloy adherends are bonded with adhesive FM73M epoxy. With increasing  $l_b$ , the debonding stress  $\sigma_c$  increases. Figure C1(b) shows the ISSF for lap joint  $K_\sigma^{E**}$  under  $\sigma^\infty = 1\text{MPa}$  by varying  $l_b$  [24]. The ISSF  $K_\sigma^{E**}$  decreases with increasing  $l_b$  in a similar way of the pull-out test and microbond test [26, 27]. Instead, under  $\sigma^\infty = \sigma_c$ , the critical ISSF  $K_{\sigma_c}^{E**}$  is almost constant independent of  $l_b$  as shown in Figure C1(c). From Figure C1, it can be conjectured that the ISSF is useful for evaluating initial debonding in pull-out test and microbond test since the adhesive strength can be expressed as a constant value as shown in Figure C1(c).